14th IEA Heat Pump Conference
15-18 May 2023, Chicago, Illinois

Numerical comparison of the yearly performance of an indirect vapour compression heat pump working with R290 with R410A systems

Nicholas Croci[a], Matteo Fusaro[a], Luca Molinaroli[a,*]

[a]Dipartimento di Energia, Politecnico di Milano, Via Raffaele Lambruschini 4/A, 20156, Milano, Italy

Abstract

In the last years, the environmental awareness is pushing the air-conditioning and refrigeration industry towards a massive use of low GWP refrigerants. Generally, despite being environmentally friendly, these new working fluids are mildly flammable, or even flammable, and therefore safety concerns arise. One possible way to cope with the flammability hazard is the reduction of the charge of the refrigerant inside the system. In this scenario, indirect systems, i.e. brine-to-water system with a remote air-to-brine heat exchanger, seem to be a viable solution since they may be built with low internal volume which, in turn, leads to a low refrigerant charge. However, the use of heat transfer fluid between the air and the refrigerant results in an increase in the energy consumption of the system, making this solution less attractive.
In the present paper, a numerical assessment of the use of R290 in an indirect expansion vapour compression system is presented. The analysed system consists of a reversible brine-to-water heat pump able to supply space heating or space cooling depending on the season. The results are compared with those of a baseline R410A system, both in direct and indirect configurations. Although the refrigerant charge is well below the maximum value currently allowed, the indirect systems show a reduction in the energy performance by around 20% with respect to the direct one.

Selection and/or peer-review under the responsibility of the organizers of the 14th IEA Heat Pump Conference 2023.

Keywords: Heat pump; Indirect expansion; R290.

1. Introduction

In the last years, the constraints introduced by the environmental regulations such as the EU 517/2014 regulation [1] and the Kigali amendment to the Montreal Protocol [2] are pushing the air conditioning and refrigeration industry is facing the transition towards the use of low-GWP refrigerants.

Among the possible options, natural refrigerants such as R290 and R744 [3] have received a lot of attention, especially in heat pump applications and/or refrigeration application and their application is becoming more and more widespread. Focusing on propane only, it has very good thermodynamic properties that may lead to high performance systems but has the drawback of flammability that may limit its diffusion. Indeed, in the open literature it is possible to find a lot of studies that deal with the reduction of the charge in propane-based systems [4-7].

In this scenario, for air-to-water heat pumps one interesting option lies in indirect expansion systems, i.e. systems in which the air is not used directly as cold heat source directly in an air-to-refrigerant evaporator, but is used in an air-to-brine heat exchanger to heat a brine flow which, in turn, acts as cold heat source in a brine-to-refrigerant evaporator. This layout leads to significant reduction in the inner volume of the refrigerant circuit, and of the refrigerant charge, which is beneficial for the system safety and risk reduction. However, some inherent energy penalization may arise since the evaporating temperature in indirect systems is generally lower than that found in direct ones because of the use on an intermediate heat transfer fluid.

* Corresponding author. Tel.: +39-02-23993872.
E-mail address: luca.molinaroli@polimi.it.

This paper wants to contribute to this general discussion presenting the results of a numerical study aimed to analyse the performance of an indirect expansion heat pump working with R290. The results are compared with those achieved by a traditional air-to-water heat pump working with R410A, which is the baseline for the comparison, and by an indirect heat pump, again operated with high-GWP refrigerant R410A.

2. Modelling

As stated, in the present study the performance of an indirect expansion heat pump is analysed and compared with that of classical air-to-water systems. Figure 1 shows the layouts of the two heat pumps considered. The main difference between the direct expansion system and the indirect one is the addition of a heat exchanger beyond the condenser-evaporator pair. Indeed, while in an air-to-water system the evaporator is a fin-and-tube coil that exchanges heat directly with the air, i.e. the cold heat source of the heat pump, in an indirect system the evaporator is a plate heat exchanger that transfers heat between the refrigerant and a secondary fluid in liquid state. This fluid, which is the "direct" cold heat source of the heat pump, is then heated in a finned coil in which a heat transfer process with air occurs. Air is then the "indirect" cold heat source of the heat pump. When the operation of the heat pump is reversed from heating to cooling, i.e. the heat pump behaves like a chiller, the secondary fluid receives heat in the plate heat exchanger, that acts as a condenser, and, in turn, rejects heat to the environmental air through the fin-and-tube heat exchanger.

The simulation model of each system is built with a bottom-up approach, i.e. connecting the sub-models of each component of the heat pump.

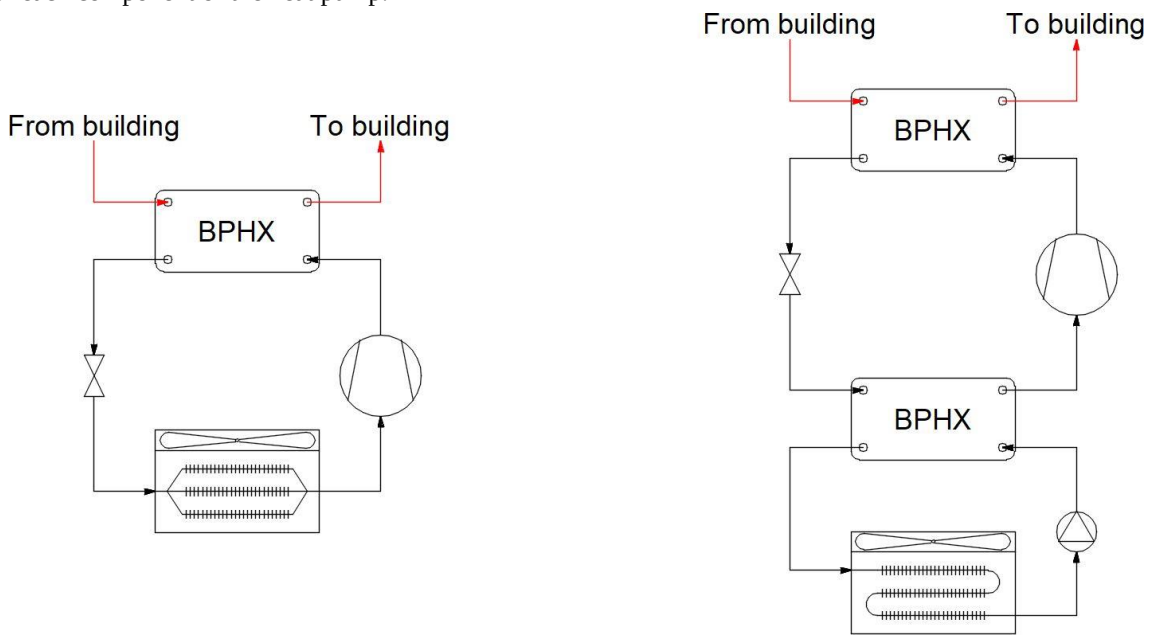

Fig. 1. Layout of the direct system (left) and indirect system (right) considered in the present study.

2.1. Compressor modelling

The compressors considered in the present study are hermetical, variable speed scroll compressors that are modelled through the ten coefficients polynomial curves that express the refrigerant mass flow rate processed by the compressor and its power consumption as per EN 12900 [8]:

$$\dot{m} = a_0 + a_1 T_{EVAP} + a_2 T_{COND} + a_3 T_{EVAP}^2 + a_4 T_{EVAP} T_{COND} + a_5 T_{COND}^2 + a_6 T_{EVAP}^3 + a_7 T_{EVAP}^2 T_{COND} + a_8 T_{EVAP} T_{COND}^2 + a_9 T_{COND}^3 \quad (1)$$

$$P = b_0 + b_1 T_{EVAP} + b_2 T_{COND} + b_3 T_{EVAP}^2 + b_4 T_{EVAP} T_{COND} + b_5 T_{COND}^2 + b_6 T_{EVAP}^3 + b_7 T_{EVAP}^2 T_{COND} + b_8 T_{EVAP} T_{COND}^2 + b_9 T_{COND}^3 \quad (2)$$

The coefficients that appear in Eqs. (1-2) are valid for a well-defined rotational speed, so different sets of coefficients are needed to compute the compressor performance when its rotational speed is changed. Finally, due to the heat pump application, the compressor is assumed to be adiabatic and, therefore, the refrigerant enthalpy at the compressor discharge is calculated through the following equation:

$$h_{DIS} = h_{SUC} + P/\dot{m} \quad (3)$$

2.2. Plate heat exchanger modelling

Plate heat exchangers models are developed using the finite volume method. Each heat exchanger is divided in small slices and the amount of heat transferred between the hot and cold fluid in the small volume is calculated using the ε-NTU method according to the following equations:

$$\varepsilon = \frac{\dot{Q}}{\dot{Q}_{MAX}} = \begin{cases} \dfrac{1 - e^{-NTU(1-R^*)}}{1 - R^* e^{-NTU(1-R^*)}} & counterflow \\ \dfrac{1 - e^{-NTU(1+R^*)}}{1 + R^*} & parallel\ flow \end{cases} \quad (4)$$

$$\dot{Q} = \dot{m}_H c_{P,H} \left(T_{H,IN} - T_{H,OUT}\right) = \dot{m}_C c_{P,C} \left(T_{C,OUT} - T_{C,IN}\right) \quad (5)$$

$$\dot{Q}_{MAX} = min\ (\dot{m}_H c_{P,H}, \dot{m}_C c_{P,C}) \left(T_{H,IN} - T_{C,IN}\right) \quad (6)$$

$$R^* = \frac{min\ (\dot{m}_H c_{P,H}, \dot{m}_C c_{P,C}) \left(T_{H,IN} - T_{C,IN}\right)}{max\ (\dot{m}_H c_{P,H}, \dot{m}_C c_{P,C}) \left(T_{H,IN} - T_{C,IN}\right)} \quad (7)$$

$$NTU = \frac{UA}{min\ (\dot{m}_H c_{P,H}, \dot{m}_C c_{P,C}) \left(T_{H,IN} - T_{C,IN}\right)} \quad (8)$$

$$(UA)^{-1} = R_H + R_{FOU,H} + R_{WALL} + R_{FOU,C} + R_C \quad (9)$$

The overall heat transfer rate is, then, the sum of the infinitesimal heat transfer rate at volume scale.

The correlation used for the calculation of the heat transfer coefficient are the correlations proposed by Longo et al. [9-10] for the evaporation, for the condensation and for the single phase fluid (water in the condenser/evaporator, secondary fluid in the evaporator/condenser, refrigerant in the vapour zone and liquid zone in the condenser and refrigerant in the vapour zone in evaporator).

The heat exchangers are designed with counterflow arrangement in the heating mode and with a parallel flow during the cooling mode.

2.3. Expansion valve modelling

The expansion valve is modelled considering an isenthalpic process and assuming that it is able to keep the superheat at the evaporator outlet at the set value of 5 K in any operating conditions.

2.4. Fin-and-tube heat exchanger modelling

The model of the fin-and-tube heat exchanger is developed using a finite volume approach [11]. Furthermore, since the flow rate of fluid is evenly divided in the exchanger circuits, it is decided to model only one circuit to reduce computational effort. Similarly to the plate heat exchangers, the heat transfer within the single element is solved by applying the ε-NTU method. Indeed, the same set of equations (5(9) is used with an update of the equation for the effectiveness calculation to account for the flow arrangement:

$$\varepsilon = \frac{\dot{Q}}{\dot{Q}_{MAX}} = \begin{cases} \frac{1}{R^*}\left(1 - e^{-R^*\left(1-e^{-NTU}\right)}\right) \; if \; (\dot{m}c_P)_{AIR} < (\dot{m}c_P)_{INN} \\ 1 - e^{-\left(1-e^{-NTU\cdot R^*}\right)/R^*} \; if \; (\dot{m}c_P)_{AIR} > (\dot{m}c_P)_{INN} \end{cases} \tag{10}$$

The correlations used for the convective heat transfer coefficient calculation are the Gnielinski correlation [12] for single phase flow inside tubes, the Diani et al. [13], for evaporation and the Kedzierski and Goncalves [14] for condensation. The air side heat transfer coefficient is calculated using the Wang et al. correlation [15] in dry mode and the Wang et al. [16] in wet mode.

Depending on the season and on the characteristics of the air, there can be different types of heat transfer (dry, wet and frost) as detailed in the next sections.

2.4.1 Dry mode: sensible heat exchange

The simplest case is related to the sensible heat transfer. In the dry mode, the surface temperature of the heat exchanger is higher than the dew point temperature of the air. The air changes its enthalpy by changing only the temperature whereas the water content, i.e. the humidity ratio, is constant. In the ε-NTU method, the dry bulb temperature is used to characterize air conditions and the Schmidt's model [17] is used to compute the fin efficiency. In the counterflow arrangement, the process to solve all the elements is iterative, since the fluids enter from two opposite sides and only the inlet temperatures are available. It is necessary to assume the outlet temperature and iterate to check the convergence. Instead, in the parallel flow, the resolution is straightforward.

2.4.2 Wet mode: latent heat exchange by air dehumidification

In the wet mode, the surface temperature of the heat exchanger is lower than the dew point temperature of the air but higher than 0 °C. In this situation, air dehumidification occurs. This phenomenon consists of the condensation of the water vapour which is in the air and it involves both the sensible heat transfer and the mass transfer (latent heat transfer).

The resolving method is the same as reported for the dry mode. However, it is necessary to modify some parameters in order to consider the mass transfer. First, the latent heat of condensation of water has to be considered in the calculation of the overall heat transfer rate as per eq. (11) in which the condensed water flow rate is computed using the mass transfer coefficient which, in turn, is estimated through the Lewis' analogy [18].

$$\dot{Q}_{LAT} = \dot{m}_{COND}\Delta h_{LV} = h_{MT}(x_{AIR} - x_{WALL})A\Delta h_{LV} \tag{11}$$

Additionally, considering that the heat transfer takes place between air and a wet surface, both the convective heat transfer coefficient and the fin efficiency change. The former is computed through an appropriate model [18] whereas the latter is modified to account for the mass transfer resistance as done in the model proposed by McQuinston et al. [18]. Finally, in order to use the ε-NTU method, the wet bulb temperature of the air must be used instead of the dry bulb temperature, which is directly connected to the air enthalpy.

2.4.3 Frost mode

In the frost mode, the surface temperature of the heat exchanger is lower than the dew point temperature of the air and, at the same time, lower than 0 °C. In this situation, frost formation and accumulation on the finned surface occurs.

In this case, the water vapour directly sublimates on the surface of the heat exchanger, passing from the gaseous state to the solid state. The heat transfer is determined by the temperature gradients between the air flow and the frost surface, while the mass transfer is determined by the vapour concentration gradients. Part of the total transferred water vapour diffuses into the existing porous frost layer, and undergoes phase transformation to ice, contributing to increase the frost density. The remainder freezes on the frost surface, contributing to increase the frost thickness [19].

Following Qiao et al. [19], the mass balance of the total water vapour transferred from the air stream to the frost layer can be expressed as:

$$\dot{m}_V = \dot{m}_\rho + \dot{m}_\delta \tag{12}$$

The sensible heat flux exchanged between the air stream and the frost surface is:

$$\dot{Q}_{SENS} = \dot{m}_{AIR} c_{P,AIR} \left(T_{AIR,IN} - T_{WALL}\right)\left(1 - e^{-UA/\dot{m}_{AIR} c_{P,AIR}}\right) \tag{13}$$

Similarly, the flow rate of vapour transferred to the surface of the exchanger is calculated as:

$$\dot{m}_V = \dot{m}_{AIR}\left(x_{AIR,IN} - x_{WALL}\right)\left(1 - e^{-h_{MT} A/\dot{m}_{AIR}}\right) \tag{14}$$

The latent heat flow due to the solidification of the vapour that freezes on the frost surface is calculated by the following equation:

$$\dot{Q}_{LAT,\delta} = \dot{m}_\delta \Delta h_{SL} \tag{15}$$

The total flux transferred during the frost formation process is given by the sum of sensible and latent contributions.

The frost formation, besides influencing the heat transfer process, also determines a variation of the fan consumption. Indeed, the frost thickness reduces the air cross-sectional area which, in turn, increases the pressure drop and changes the operating point of the fan. The new operating point, that changes over time as frost accumulates, has typically a lower flow rate and a higher power consumption.

In order to remove the frost, bringing the finned surface back to the initial, frost-free condition, defrosting cycles are designed. Two main issues are considered: the defrosting time and defrosting cycle frequency. The defrosting time is the period required to ensure the correct melting of the frost accumulated on the surface. The value is proportional to the mass of ice, which can be calculated as:

$$M_F = \rho_F A \delta_F \tag{16}$$

While the energy needed to melt the frost mass is:

$$E_F = M_F \Delta h_{SL} \tag{17}$$

For the sake of simplicity, a constant defrosting time equal to 300 s is assumed.

On the other hand, the choice of the defrost frequency is essential to ensure proper heat pump operation. Indeed, too infrequent defrosting cycles lead to the formation of large thicknesses of ice on the surface, while too frequent defrosting involves waste of energy. To accurately define the correct defrost start time, the defined thickness should be evaluated instantaneously. However, the frost thickness is difficult to measure, so, the defrost frequency is set on the excess of the fan pressure increase that arises from the increase of air pressure drop. Indeed, once the maximum value of the pressure increase is reached, the operation of the fan is stopped and the 300 s defrosting cycle starts.

3. Case study description

3.1. Building

The building considered in the present study is taken from the scientific literature [20]. It is a new single-family house that consists of two levels with a floor area of 70 m^2 each. Radiant floor is considered as the indoor emitting system. The main feature of the building are reported in Table 1.

Table 1. Main feature of the building

U_{WALL}	0.15 W/(m^2K)
U_{ROOF}	0.13 W/(m^2K)
U_{FLOOR}	0.15 W/(m^2K)
$U_{WINDOWS}$	1.10 W/(m^2K)
U_{DOOR}	1.30 W/(m^2K)
$\Delta U_{THERMAL\ BRIDGE}$	0.05 W/(m^2K)
Infiltration	0.10 h^{-1}
Ventilation System	Yes

The thermal loads are calculated in TRNSYS environment and considering the two levels as a single thermal zone. From the annual simulation, the maximum heating load is equal to 6340 W (T_{AIR} = -12 °C) while the maximum cooling load is equal to 6317 W (T_{AIR} = 32 °C). For the sizing of the heating/cooling system, these values are "rounded" to reproduce a slight oversizing that would be found in a real application. The building is characterized by a heating period longer than the cooling period. For this reason, the system works mainly as a heat pump. The guideline used to choose the components is to prefer and guarantee the maximum efficiency in winter conditions. As a result, the nominal conditions on which the systems are designed are: T_{AIR} = -12 °C, $\dot{Q}_{BUILDING}$ = 7000 W, duration of heating season equal to 2822 h.

3.2. Heat pump

In the present study, three different heat pumps are considered:

- The first heat pump is an air-to-water heat pump working with R410A. This heat pump allows for the direct installation and, therefore, is considered as the current, largely diffused baseline technology.
- The second heat pump is a water-to-water heat pump working with R410A. This heat pump allows for indirect installation. It is considered as the term of comparison for indirect systems.
- The third heat pump is a water-to-water heat pump working with R290. This heat pump works with propane and is used in indirect installation with the aim of reducing refrigerant charge. It is the innovative system in indirect systems.

Air-to-water heat pump working with R290 is not considered in the present study since it requires a large refrigerant charge.

The R410A air-to-water heat pump is sized considering the constraint shown in **Error! Reference source not found.**. On the other side, considering the water-to-water heat pumps, to allow them to work even when the outside air temperature drops below 0 °C, a mixture of water and ethylene glycol is chosen as secondary fluid to avoid mixture freezing. The glycol concentration is set to 40% so that the freezing temperature is -24.8 °C whereas the inlet and outlet design temperatures are -20 °C and -17 °C respectively since the minimum air temperature is -12 °C.

All the three heat pumps are sized considering real, commercially available components. The characteristics of the main components of the three heat pumps considered are collected in Table 2.

Table 2. Main characteristics of the components of the three heat pumps

Component	Air-to-water R410A	Water-to-water R410A	Water-to-water R290
Compressor	Scroll compressor	Scroll compressor	Scroll compressor

	Variable speed	Variable speed	Variable speed
	Swept volume: 25 cm^3/rev	Swept volume: 25 cm^3/rev	Swept volume: 45 cm^3/rev
	Rotational frequency: 35 Hz – 110 Hz	Rotational frequency: 35 Hz – 110 Hz	Rotational frequency: 35 Hz – 110 Hz
	Oil charge: 0.74 dm^3	Oil charge: 0.74 dm^3	Oil charge: 1.45 dm^3
Condenser	Plate height: 526 mm	Plate height: 526 mm	Plate height: 526 mm
(plate heat exchanger)	Plate width: 119 mm	Plate width: 119 mm	Plate width: 119 mm
	Plate pitch: 1.56 mm	Plate pitch: 1.56 mm	Plate pitch: 1.56 mm
	φ = 1.24	φ = 1.24	φ = 1.24
	Plate number: 18	Plate number: 18	Plate number: 18
Evaporator	Tube inner diameter: 9.52 mm	-	-
(fin-and-tube heat exchanger)	Tube outer diameter: 10.12 mm		
	Tube length: 1000 mm		
	Transversal pitch: 25 mm		
	Longitudinal pitch: 21.65 mm		
	Fin pitch: 4.2 mm		
	Fin thickness: 0.15 mm		
	Number of tubes: 40		
	Number of rows: 4		
	Number of circuits: 4		
Evaporator	-	Plate height: 526 mm	Plate height: 526 mm
(plate heat exchanger)		Plate width: 119 mm	Plate width: 119 mm
		Plate pitch: 1.56 mm	Plate pitch: 1.56 mm
		φ = 1.24	φ = 1.24
		Plate number: 24	Plate number: 22
Finned coil		Tube inner diameter: 9.52 mm	Tube inner diameter: 9.52 mm
(indirect evaporator)		Tube outer diameter: 10.12 mm	Tube outer diameter: 10.12 mm
		Tube length: 810 mm	Tube length: 810 mm
		Transversal pitch: 25 mm	Transversal pitch: 25 mm
		Longitudinal pitch: 21.65 mm	Longitudinal pitch: 21.65 mm
		Fin pitch: 4.2 mm	Fin pitch: 4.2 mm
		Fin thickness: 0.15 mm	Fin thickness: 0.15 mm
		Number of tubes: 32	Number of tubes: 32
		Number of rows: 4	Number of rows: 4
		Number of circuits: 8	Number of circuits: 8

It is worth mentioning that the compressor for R290 is not a native variable speed compressor. However, for the sake of homogenous comparison, in the present study it is assumed that it is possible to drive it through an inverter. In order to compute the compressor performance at rotational speed different from 50 Hz, corrective look-up tables are prepared starting from the data available with the R410A, variable speed compressor. Tables that report the refrigerant mass flow rate and compressor power consumption as a function of the shaft rotational frequency and in broad ranges of evaporating and condensing temperatures are first generated and, then, normalised considering the nominal rotational frequency equal to 50 Hz. This results in correction coefficients that represent the reduction (increase) in the refrigerant mass flow rate or compressor power as a result of the reduction (increase) in the shaft rotational frequency. These values are applied to the R290 compressor to simulate its behaviour under variable speed regime.

The heat pumps sizing is then completed with the estimation of the refrigerant charge. The amount of refrigerant which is contained in each component is computed dividing the inner volume by the refrigerant specific volume. More in detail, for the components in which the refrigerant is in single phase, i.e. compressor, pipes, desuperheating zone and subcooling zone of the condenser and superheating zone of the evaporator, the specific volume is calculated considering the average inlet-outlet pressure and temperature. On the other hand, for the components in which the refrigerant undergoes a phase change, i.e. the condensing

zone of the condenser and the evaporating zone of the evaporator, the average specific volume is computed starting from those of the saturated liquid and saturated vapour and using the void fraction models proposed by Steiner [21] in the fin-and-tube heat exchanger and by Smith [22], as suggested by Mancini [23], in the plate heat exchangers. Finally, refrigerant mass trapped in the oil is accounted for considering the solubility diagram of the refrigerant-oil pair that is provided by the compressor manufacturer. Overall, the refrigerant charge in the R410A air-to-water heat pump is estimated to be 3561 g. This value is 20% lower than that of a real air-to-water heat pump of similar capacity which, as per the manufacturer's catalogue, is filled with 4320 g of R410A [24]. However, it must be mentioned that the calculation of the charge does not consider any liquid receiver which, in turn, is installed in the real heat pump. As a result, it is possible to state that the charge calculation is quite accurate. For the water-to-water heat pumps, the refrigerant charge is estimated in 899 g with R410A and in 467 g with R290. The water-to-water heat pump has a lower internal volume with respect to the air-to-water one since the fin-and-tube evaporator is replaced by a plate heat exchanger. As a result, the refrigerant charge of R410A reduces by 75%. The charge of the R290 heat pump is even lower since the density of R290 is significantly lower than that of R410A in the full set of operating conditions.

Finally, pumps and fans used to supply the secondary fluid flow rate are chosen. The main characteristics of these devices are reported in Table 3.

Table 3. Main characteristics of the pumps and fans

Component	Air-to-water R410A	Water-to-water R410A	Water-to-water R290
Pump (end-user side)	Not considered since it is the same in each system	Not considered since it is the same in each system	Not considered since it is the same in each system
Fan (fin-and-tube evaporator)	Air flow rate: 6386 m^3/h Power consumption: 293 W	-	-
Pump (plate evaporator	-	Water flow rate: 1.8 m^3/h Power consumption: 115 W	Water flow rate: 1.8 m^3/h Power consumption: 119 W
Fan (indirect evaporator)	-	Air flow rate: 7712 m^3/h Power consumption: 628 W	Air flow rate: 7712 m^3/h Power consumption: 628 W

3.3. Seasonal simulation and performance index

The analysis of the performance of the three heat pumps is carried out considering one year of operation. The yearly simulation is carried out considering a time step equal to 3600 s and assuming that the heat pump operates in steady state regime in it. If frost formation occurs, the time step is reduced to 300 s but, again, the heat pump is assumed to work in steady state in the time step while it changes its operating point from one time step to the other.

At each time step the building load is available from the building simulation whereas the heat pump heating capacity is computed from the simulation tool. Since each heat pump is built with a variable speed compressor, the matching between the end-user need and the capacity delivered by the heat pump may occur by varying the rotational frequency of the compressor shaft, or by on-off cycling. In the former situation, the compressor speed is changed so that the heat pump delivers exactly the building load; in this scenario, the heat pump is assumed operate continuously for the full time step. On the other hand, in the latter situation, which typically occurs at high ambient temperatures, despite the compressor speed is set to the minimum value, the heat pump capacity is higher than the building load and, so, it undergoes on-off cycling with the aim of providing a time step average capacity equal to the building energy need. This working condition is not optimal since additional power consumption related to electronic board arises even when the compressor is switched off. To account for it, a correction of the COP as proposed by EN 14825 [25] is used:

$$COP_{ON-OFF} = \frac{CR}{1 - C_D + C_D \cdot CR} COP_{CONTINUOS} \quad (18)$$

In eq. (18) CR is the capacity ratio, i.e. the ratio between the building load and the heat pump capacity, whereas C_D is the degradation coefficient for on-off cycling, equal to 0.9, and $COP_{CONTINUOS}$ is the coefficient of performance of the heat pump that operates without on-off cycling. It is worth specifying that the control of the heat pump capacity is achieved acting simply on the rotational frequency of the compressor shaft. All the other components that may vary their rotational speed, i.e. the fan of the evaporator for the

direct system and the fan of the air-to-glycol heat exchanger and the glycol pump for the indirect ones, are instead kept at the maximum speed.

Overall, the performance indexes that are used to compare the three different heat pumps are the seasonal coefficient of performance and the Total Equivalent Warming Impact ($TEWI$) that are calculated as follows:

$$SCOP = \frac{\sum_{i=1}^{n} \dot{Q}_{BUILDING,i} \Delta t}{\sum_{i=1}^{n} \left(P_{COMP,i} + P_{PUMP,i} + P_{FAN,i} + P_{DEFROST,i}\right) \Delta t} \tag{19}$$

$$TEWI = \alpha_{LEAK} M_{REF} nGWP + (1 - \varepsilon_{REC}) M_{REF} GWP + E_{EL} n M_{CO_2} \tag{20}$$

4. Results

Starting from, the energy performance index, Fig. 2 shows the $SCOP$ and the $SCOP_{HP}$ of the three different heat pumps considered in the present study. $SCOP$ is defined as per Eq. (19) and accounts for the power consumption of the compressor, the auxiliaries and the defrost, whereas the $SCOP_{HP}$ is the Seasonal Coefficient Of Performance of the heat pump only, i.e. it accounts for the compressor consumption only. The rationale behind these indexes is pointing out the differences that arise not only from the system layout, i.e. direct and indirect, but also to highlight the performance of the use of different refrigerants.

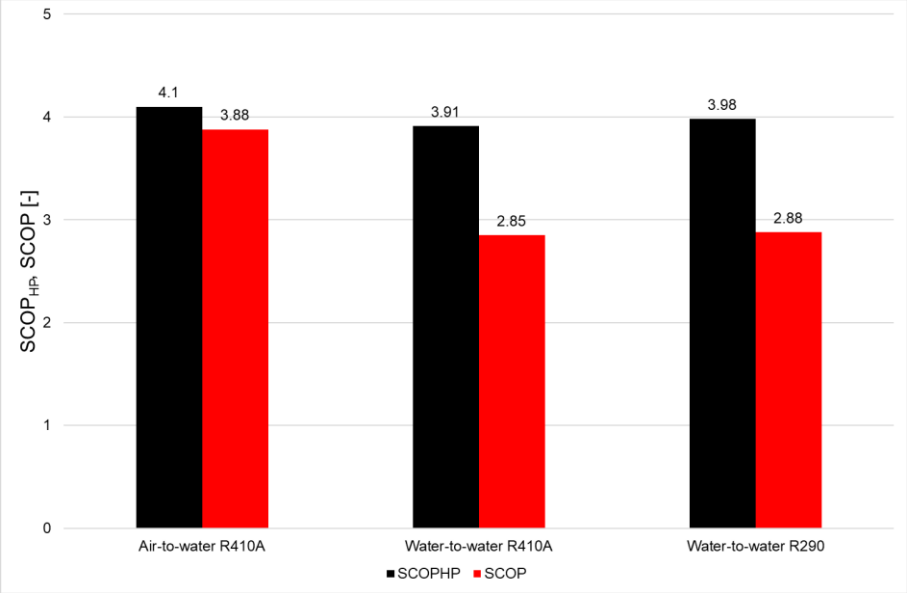

Fig. 2. $SCOP_{HP}$ and SCOP of the three systems.

From the analysis of the figure, it is possible to conclude that the performance of the heat pump only is very similar since a reduction in the $SCOP_{HP}$ of around 3% is found passing from direct R410A system to indirect ones. Additionally, in indirect systems a slight tendency of R290 to perform better than R410A may be found because the $SCOP_{HP}$ of the heat pump that uses the natural refrigerant is around 2% higher than that of R410A-based heat pump. However, a significant difference arises when the consumptions related to the auxiliaries and the defrosting cycles are taken into consideration. Indeed, the $SCOP$ of the overall system is around 26% lower for the indirect heat pumps with respect to the direct one. This is related to the strong increase in the fan and pump consumptions that arises in the indirect systems. Indeed, as shown in **Error! Not a valid bookmark self-reference.**, in these systems the fan consumption is around 5 times higher than the fan consumption in direct system and also the consumption of the water-ethylene glycol mixture is not negligible since it is even higher than the consumption of the fan of direct systems. The first result is not surprising: in indirect system, the evaporating temperature is significantly lower than the air temperature since heat is extracted from the water-ethylene glycol mixture which, in turn, is colder than air. As a result, in indirect systems there is an increase in the range of air temperature and humidity conditions in which the frost formation and accumulation phenomenon occurs. This result in an increase in the air side pressure drop

which, in turn, leads to an increase in the fan consumption. Similarly, although the pump power consumption is small, the large number of operating hours, i.e. the full heating season, leads to a not negligible energy consumption.

Table 4. Details on energy consumption of the three heat pumps

	Fan	Pump
Air-to-water R410A	122.5 kWh	-
Water-to-water R410A	670.9 kWh	202.4 kWh
Water-to-water R290	674.4 kWh	204.6 kWh

Finally, the $TEWI$ of the three systems is in Fig. 3. For the calculation of this environmental index, the GWP values are taken from the last IPCC report [26] resulting in GWP_{100} = 0.02 and GWP_{100} = 2256 for R290 and R410A respectively. The refrigerant leakage is assumed to be 2% and, additionally, it is assumed that it does not influence the heat pump performance. This may be a source of error, especially for indirect systems that might not be built with liquid receiver, but it is done for the sake of simplicity since the model developed for this study is not able to simulate the operation of a heat pump in undercharged conditions. The other parameters are: lifetime of the system equal to 10 years, end-of-life recovery efficiency 90% and emission of CO_2 per unit of electrical energy 247 g/kWh [27]. Comparing the results, it is possible to state that, despite its lower energy performance, the system using R290 largely benefits from the low-GWP of this refrigerant since its $TEWI$ is around 5% lower than that of the baseline solution despite its higher energy consumption. On the other hand, comparing the two systems working with R410A, the indirect one has a lower direct impact, as a consequence of the lower charge, but higher indirect emission since it shows higher energy consumption. Overall, the two effects approximately compensate each other resulting in a $TEWI$ only around 4% higher than that of the baseline system.

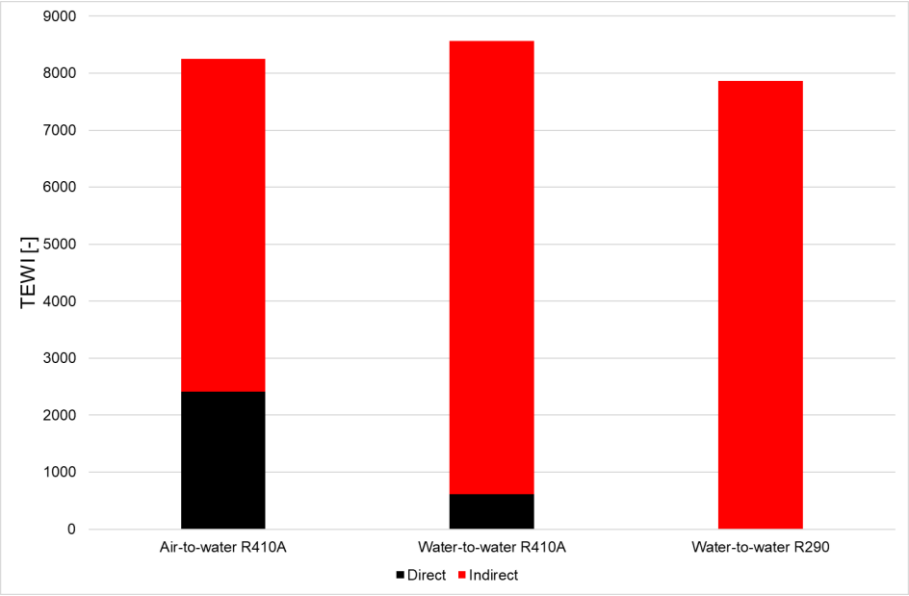

Fig. 3. TEWI of the three systems.

5. Conclusions

In the present paper, the performance of an indirect expansion heat pump working with R290 is analysed and compared with that of R410A heat pumping systems. For this refrigerant, both well-established air-to-water heat pump, i.e. direct system, and water-to-water heat pump, i.e. indirect system, are considered.

The analysis is carried out on a yearly basis using a simulation tool designed and built for this purpose. Seasonal coefficient of performance ($SCOP$) is used as energy performance index whereas total equivalent warming impact ($TEWI$) is used to measure the equivalent carbon dioxide emissions of the three systems.

Overall, the direct system performs better than the indirect ones both from the energy efficiency point of view and the environmental point of view. Indeed, the $SCOP$ of the indirect systems are around 25% lower than that of the direct system whereas the $TEWI$ is around 9%-15% higher. However, the refrigerant charge in indirect system is significantly lower than that required in a direct system, resulting in an improvement in the system safety.

Nomenclature

$a_0 \dots a_9$	Coefficients in eq. (1)
A	Area [m^2]
$b_0 \dots b_9$	Coefficients in eq. (2)
c_P	Isobaric heating capacity [J/(kg·K)]
C_D	Degradation coefficient [-]
COP	Coefficient of performance [-]
CR	Capacity ratio [-]
E	Energy [J]
GWP	Global warming potential [-]
h	Enthalpy [J/kg]
h_{MT}	Mass transfer coefficient [kg/(m^2·s)]
M	Mass [kg]
M_{CO_2}	Emission of carbon dioxide per unit of energy [kg/kWh]
$\dot{m}$	Mass flow rate [kg/s]
$\dot{m}_\rho$	Mass flow rate of vapour that increases the frost density [kg/s]
$\dot{m}_\delta$	Mass flow rate of vapour that increases the frost thickness [kg/s]
n	Number of years [-]
NTU	Number of Transfer Unit [-]
P	Power [W]
$\dot{Q}$	Heat transfer rate [W]
R	Thermal resistance [K/W]
R^*	Heat capacity ratio [-]
$SCOP$	Seasonal coefficient of performance [-]
T	Temperature [K]
$TEWI$	Total equivalent warming impact [kg]
U	Overall heat transfer coefficient [W/K]
x	Humidity ratio [kg/kg$_{DA}$]
Greek symbols	
α_{LEAK}	Leakage rate [-]
δ	Thickness [m]
Δh_{LV}	Liquid-to-vapour phase change enthalpy [J/kg]
Δh_{SL}	Solid-to-liquid phase change enthalpy [J/kg]
Δt	Time step [s]
ε	Effectiveness [-]
ε_{REC}	Recovery efficiency [-]
ρ	Density [kg/m^3]

Subscript			
AIR	Air	*FOU*	Fouling
BUILDING	Building	*H*	Hot
C	Cold	*IN*	Inlet
COMP	Compressor	*INN*	Inner
COND	Condensing	*LAT*	Latent
DEFROST	Defrost	*PUMP*	Pump
DIS	Discharge	*REF*	Refrigerant
EL	Electrical	*SENS*	Sensible
EVAP	Evaporating	*SUC*	Suction
F	Frost	*V*	Vapour that frosts
FAN	Fan	*WALL*	Wall

References

[1] European Union , 2014. Regulation (EU) no 517/2014 of the european parliament and the EU Council of 16 april 2014 on fluorinated greenhouse gases and repealing Regulation (EC) no 842/2006. Off. J. Eur. Union 150, 195–230.
[2] United Nations, 2016. The amendment to the Montreal Protocol agreed by the Twenty-Eighth Meeting of the Parties (Kigali, 10–15 October 2016).
[3] Tammaro, M., Montagud, C., Corberán, J.M., Mauro, A.W., Mastrullo, R., 2017. Seasonal performance assessment of sanitary hot water production systems using propane and CO2 heat pumps. International Journal of Refrigeration 74, pp. 224-239.
[4] Fernando, P., Palm, B., Lundqvist, P., Granryd, E. Propane heat pump with low refrigerant charge: design and laboratory tests. International Journal of Refrigeration 27, pp. 761-773.
[5] Corberán, J.M., Martínez, I.M., Gonzálvez, J. Charge optimisation study of a reversible water-to-water propane heat pump. International Journal of Refrigeration 31, pp. 716-726.
[6] Cavallini, A., Da Riva, E., Del Col, D., Performance of a large capacity propane heat pump with low charge heat exchangers. International Journal of Refrigeration 33, pp. 242-250.
[7] Ghoubali, R., Byrne, P., Bazantay, F., 2017. Refrigerant charge optimisation for propane heat pump water heaters. International Journal of Refrigeration 76, pp. 230-244.
[8] European Committee for Standardization, 2013. EN 12900 - Refrigerant compressors - Rating conditions, tolerances and presentation of manufacturer's performance data.
[9] Longo, G.A., Mancin, S., Richetti, G., Zilio, C., 2015. A new model for refrigerant boiling inside Brazed Plate Heat Exchangers (BPHEs). International Journal of Heat and Mass Transfer 91, pp. 144–149.
[10] Longo, G.A., Richetti, G., Zilio, C., 2015. A new computational procedure for refrigerant condensation inside herringbone-type Brazed Plate Heat Exchangers. International Journal of Heat and Mass Transfer 82, pp. 530–536.
[11] Joppolo, C.M., Molinaroli, L., Pasini, A., 2015. Numerical analysis of the influence of circuit arrangement on a fin-and-tube condenser performance. Case Studies in Thermal Engineering 6, pp.136-146.
[12] Gnielinski, V., 2013. On heat transfer in tubes. International Journal of Heat and Mass Transfer, 63, pp. 134-140.
[13] Diani, A., Mancin, S., Rossetto, L., 2014. R1234ze(E) flow boiling inside a 3.4 mm id microfin tube. International Journal of Refrigeration 47, pp. 105-119.
[14] Kedzierski, M.A., Goncalves, J.M., 1999. Horizontal convective condensation of alternative refrigerants within a micro-fin tubes. Enhanced Heat Transfer 6, pp. 161-178.
[15] Wang, C.-C., Lee, C.-J., Chang, C.-T., Lin, S.-P., 1999. Heat transfer and friction correlation for compact louvered fin-and-tube heat exchangers. International Journal of Heat and Mass Transfer 42, pp. 1945-1956.
[16] Wang, C.-C., Lin, Y.-T., Lee, C.-J., 2000. Heat and momentum transfer for compact louvered fin-and-tube heat exchangers in wet conditions. International Journal of Heat and Mass Transfer 43, pp. 3443-3452.
[17] Schmidt, T.E., 1949. Heat transfer calculations for extended surfaces. Refrigerating engineering, pp. 351-357.
[18] Mc Quiston, F.C., Parker, J.D., Spitler, J.D. Heating, ventilating, and air conditioning: analysis and design. John Wiley & Sons, 2004.
[19] Qiao, H., Aute, V., Radermacher, R., 2017. Dynamic modeling and characteristic analysis of a two-stage vapor injection heat pump system under frosting conditions. International Journal of Refrigeration 84, pp. 181-197.
[20] Scoccia, R., Toppi, T., Aprile, M., Motta, M., 2018. Absorption and compression heat pump systems for space heating and dhw in european buildings: Energy, environmental and economic analysis. Journal of Building Engineering 16, pp. 94-105.
[21] Steiner, D., 1993. Heat transfer to boiling saturated liquids. VDI Heat Atlas
[22] Smith, S.L., 1969. Void fraction in two-phase flow: a correlation based upon an equal velocity head model. Proceedings of the Institution of Mechanical Engineers 184, 647-664
[23] Mancini, R., 2019. Design and performance analysis of plate heat exchangers for heat pumps using pure and mixed refrigerants. PhD thesis, Danish Technical University.
[24] Aermec, ANK 020-085 Installation manual.
[25] European Committee for Standardisation, 2018.EN 14825 - Air conditioners, liquid chilling packages and heat pumps, with electrically driven compressors, for space heating and cooling - Testing and rating at part load conditions and calculation of seasonal performance
[26] IPCC, 2022: Climate Change 2022: Impacts, Adaptation and Vulnerability. Contribution of Working Group II to the Sixth Assessment Report of the Intergovernmental Panel on Climate Change. Cambridge University Press. Cambridge University Press, Cambridge, UK and New York, NY, USA, 3056 pp.
[27] European Environment Agency, 2022. https://www.eea.europa.eu/data-and-maps/daviz/co2-emission-intensity-12/#tab-chart_2.